IEEE Access
Multidisciplinary ⋮ Rapid Review ⋮ Open Access Journal

Received 28 July 2023, accepted 15 August 2023, date of publication 1 September 2023, date of current version 8 September 2023.

Digital Object Identifier 10.1109/ACCESS.2023.3311265

RESEARCH ARTICLE

Power Consumption Model Construction and Analysis for Soft Synchronization FMCW Radar

PING LI[1,2] AND TAO WANG[3], (Senior Member, IEEE)

[1]School of Electronics and Information, Hangzhou Dianzi University, Hangzhou 310018, China
[2]Zhejiang Provincial Key Laboratory of Equipment Electronics, Hangzhou 310018, China
[3]Shanghai Institute for Advanced Communication and Data Science, Key Laboratory of Specialty Fiber Optics and Optical Access Networks, Joint International Research Laboratory of Specialty Fiber Optics and Advanced Communication, Shanghai University, Shanghai 200072, China

Corresponding author: Ping Li (pingli@hdu.edu.cn)

This work was supported in part by the National Natural Science Foundation of China under Grant 62171170, and in part by the Central Guiding Local Science and Technology Development Fund Projects of China under Grant 2023ZY1008.

ABSTRACT Soft synchronization frequency modulated continuous wave (SS-FMCW) radars not only have the diversity of transmit signals, but also have the flexibility of hardware structure. This article proposes a power consumption model for further analyzing the power performance of the SS-FMCW radar, which is a module-level model designed for intermittent ramp signals. First, based on the principle behind the SS-FMCW radar, we build the power consumption model of the radar transmitter and receiver according to the characteristics of intermittent ramp signals. Second, to analyze the power consumption performance of the SS-FMCW radar, we propose a duty cycle factor. In addition, we compare the power consumption performance of traditional frequency modulated continuous wave (FMCW) radar and the SS-FMCW radar with different factor values through theoretical analysis. Finally, the rationality of the theoretical analysis is verified by simulation experiments and actual test experiments. The experimental results show that the SS-FMCW radar has obvious advantages in power consumption performance compared with the traditional FMCW radar. Specifically, when $D_p = 0.5$, compared with the traditional FMCW radar, the power consumption of the SS-FMCW radar is reduced by 18.6% in the actual test experiments.

INDEX TERMS Power consumption model, soft synchronization frequency modulated continuous wave (SS-FMCW) radar, intermittent ramp signals, duty cycle factor.

I. INTRODUCTION

A. BACKGROUND

The devices used for hand gesture recognition (HGR) and human motion recognition (HMR) mainly include cameras, radars and wearable sensors. Then, the research on HGR and HMR based on frequency-modulated continuous wave (FMCW) radar has gained more and more attention with the emphasis on privacy protection [1], [2], [3], [4], [5], [6], [7], [8], [9], [10], [11]. However, the traditional FMCW radar hardware structure is relatively fixed and the slope signal is relatively single, so it lacks diversity. Flexible adaptation of the radar hardware architecture and ramp signals to different application scenarios is difficult. For this problem, in the previous work [12], [13], we proposed a soft synchronization frequency modulated continuous wave (SS-FMCW) radar, which is an improved FMCW radar with structural flexibility and signal diversity. Specifically, the SS-FMCW radar adopts a software synchronization method to get rid of the hardware synchronization signal link. It saves the system overhead caused by hardware synchronization signal generation, transmission and acquisition, then improves the flexibility of radar hardware structure design. Furthermore, the basic types of intermittent ramp signals include intermittent sawtooth signals and intermittent triangular wave signals. The waveform of the transmit signal can be flexibly adjusted to suit different application scenarios by setting different time intervals, periods, and slopes. However, the research on this radar is not deep enough to show its advantages in power consumption performance. Therefore, in this work, we will model the power consumption of the SS-FMCW radar, and improve the power consumption performance of the radar by setting the relevant parameters of the ramp signals.

The associate editor coordinating the review of this manuscript and approving it for publication was Wei Wei.

This work is licensed under a Creative Commons Attribution-NonCommercial-NoDerivatives 4.0 License.
For more information, see https://creativecommons.org/licenses/by-nc-nd/4.0/

B. RELATED WORK

Many scholars have made a significant contribution to the research on radar power consumption [14], [15], [16], [17], [18], [19], [20], [21], [22], [23]. For example, Shi et al. [16] address the problem of designing the joint sub-carrier selection and power allocation scheme to minimize the power consumption of a dual function radar communications system. The key is to select the best possible sub-carriers for radar and communications purposes in sequence and allocate the optimal power resources on the corresponding sub-carrier under the constraints of mutual information of target characteristics and information transmission rate. Finally, the effectiveness of the theoretical analysis and the proposed joint optimization scheme are verified by numerical experiments. Zhang et al. [18] propose an efficient power allocation strategy for the multiple input multiple output (MIMO) radar maneuvering target tracking. The mechanism of the strategy is to achieve the optimal acquire based on the target maneuver prior to information during the tracking period. Then, they drive the predicted conditional Cramer-Rao lower bound as an optimization criterion. Using the monotone decreasing property of the objective function, they propose an efficient solver based on sequence relaxation. Simulation results show that this strategy has better tracking performance than a uniform distribution.

Based on deep reinforcement learning, Shi et al. [20] propose a data-driven multi-radar system target tracking resource allocation method. The goal is to minimize the long-term and short-term power consumption of the system through radar selection and multi-target power allocation under the premise of meeting the given tracking accuracy requirements. To solve this problem, they propose a constraint of deep reinforcement learning based on depth deterministic strategy gradient. Considering the limited radar and power resources, they redesign the three-layer output layer of the actuator network to determine the actions of radar selection and power allocation. The final simulation results show the effectiveness of this method. Tian et al. [22] study the power distribution for the orthogonal frequency division multiplexing (OFDM) based dual-function radar and communication sensor. Specifically, the signal-to-noise (SNR) ratio of the radar is taken as the optimization objective, and the word error probability and total transmission power are taken as the constraints. Then, they propose an alternative direction sequential relaxation programming algorithm, which can transform the original non-convex problem into an approximate convex problem. The final simulation results show that, compared with the average power allocation, this scheme can improve the SNR of radar.

In the previous work [12], we design an efficient, flexible and low-cost FMCW radar platform based on the scheme of analog components. This platform can quickly and flexibly generate waveforms that meet the measurement requirements and significantly improve the experimental efficiency. The signal waveform of the platform is flexible, but its hardware structure lacks flexibility. To this problem, we design the SS-FMCW radar in the subsequent work [13], which not only has the diversity of signal design, but also gets rid of hardware synchronous signal link. Then, we verify the scientific and effectiveness of the radar through theoretical analysis and practical testing. Furthermore, in the subsequent work [24], we propose a four-threshold frequency band variance synchronization algorithm, which further improves the soft synchronization performance of the SS-FMCW radar. The accurate detection of the starting points is the guarantee of the range, speed and micro Doppler information acquisition. In addition, in the subsequent work [25], we explore the power optimization strategy under the constraints of soft synchronization performance and radar ranging performance, i.e., the soft synchronization constrained energy efficiency (SSC-EE) strategy.

However, the modeling and analysis of the SS-FMCW radar power consumption are not deep enough, and there is no detailed comparison with the traditional FMCW radar. In the previous work, we have described the advantages of the SS-FMCW radar in signal diversity and hardware structure flexibility compared with the traditional FMCW radar, but we have not made further analysis of the power consumption performance of both. There is still a gap in this part of the research.

C. OUR CONTRIBUTION

Through the above analysis, this paper proposes a module-level radar power consumption model for intermittent ramp signals and analyzes the power consumption performance of the SS-FMCW radar based on the duty cycle factor, i.e., D_p, which is the ratio of T_1 to T. In short, we make contributions as follows.

1) We analyze the power consumption of each component of the transmitter and receiver of the SS-FMCW radar, then propose a module-level power consumption model for intermittent ramp signals.
2) To facilitate the power consumption performance analysis of the SS-FMCW radar, we propose the duty cycle factor. As well as, we explore the relationship between its different values and the power consumption performance of the radar.
3) Experimental results show that the SS-FMCW radar has advantages in power consumption performance compared to the traditional FMCW radar.

The rest of this article is structured as follows. Section II introduces the principle of the SS-FMCW radar based on intermittent ramp signals. Section III introduces the module-level power consumption model of the SS-FMCW radar. Section IV introduces the duty cycle factor and makes a theoretical analysis. Section V introduces the experimental equipment and results. Section VI concludes this article.

II. PRINCIPLE OF THE SS-FMCW RADAR

Compared with the traditional FMCW radar, the SS-FMCW radar not only has the diversity of transmit signals, but also has the flexibility of hardware structure. Specifically, the traditional ramp signals are usually sawtooth wave signals and triangle wave signals, which are relatively fixed and single. Based on the traditional ramp signals, we draw on the concept of sparsity and then construct intermittent ramp signals, which include intermittent triangular wave signals and intermittent sawtooth wave signals. In this paper, the intermittent triangle wave signal is taken as an example for analysis, and the waveform diagram is shown in Fig. 1. The abscissa of the graph is time, and the ordinate is frequency.

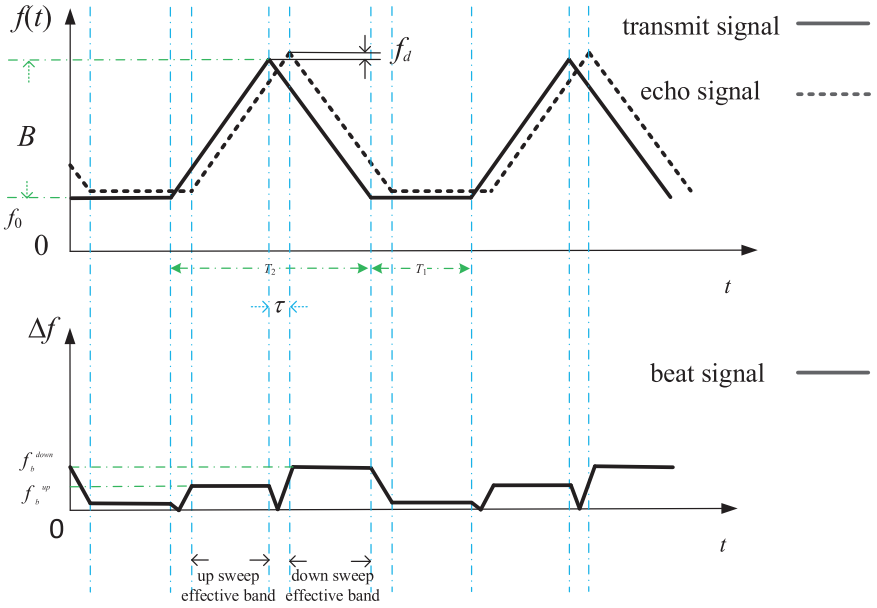

FIGURE 1. Schematic diagram of the mixing process of radar transmit signal and echo signal.

According to the upper part of Fig. 1, we know that the period of the intermittent triangular wave signal is $T = T_1+T_2$, where, T_1 is the duration of a direct current (DC) part and T_2 is the duration of a triangular part. Furthermore, the beat signal is shown in the lower part of Fig. 1. To explain the principle of the SS-FMCW radar more clearly, the mixing process of transmit signal and echo signal will be described mathematically [26].

As an example, the transmit signal of the SS-FMCW radar is shown in Formula (1), as shown at the bottom of the next page, where, A_0, f_0, B, $k = 2B/T_2$ and φ_0 are amplitude, initial frequency, bandwidth, frequency modulation slope and initial phase of the transmit signal, respectively.

Assume that the initial position of the target is R_0 from the radar, and the target moves at a uniform speed v towards the radar. Thus, the time delay can be expressed as $\tau(t) = 2(R_0 - vt)/c$, and the echo signal of the target is shown in Formula (2), as shown at the bottom of the next page, where, K_r represents the reflection coefficient of the target, and φ_r represents the phase change caused by reflection.

For the convenience of description, this paper will take the mixing process of the upper sweep part of the first cycle as an example, which can be expressed as

$$\begin{aligned} s_b^{up}(t) &= s_t^{up}(t) * s_r^{up}(t) \\ &= A_0 \cos\{2\pi[f_0(t-T_1) + \frac{k}{2}(t-T_1)^2] + \varphi_0\} \\ &\quad \times K_r A_0 \cos\{2\pi[f_0(t-\tau(t)-T_1) \\ &\quad + \frac{k}{2}(t-\tau(t)-T_1)^2] + \varphi_0 + \varphi_r\} \\ &= \frac{1}{2}K_r A_0^2\{\cos[2\pi(2f_0 t - 2f_0 T_1 \\ &\quad - f_0\tau(t) + \frac{k}{2}(2t^2 + 2T_1^2 + \tau(t)^2 \\ &\quad - 4T_1 t - 2\tau(t)t + 2\tau(t)T_1)) + 2\varphi_0 + \varphi_r] \\ &\quad + \cos[2\pi(f_0\tau(t) - \frac{k}{2}(\tau(t)^2 \\ &\quad - 2\tau(t)t + 2\tau(t)T_1)) - \varphi_r]\} \end{aligned} \tag{3}$$

where, $s_t^{up}(t)$ represents the upper sweep part of the first cycle of the transmit signal, and $s_r^{up}(t)$ represents the upper sweep part of the first cycle of the echo signal. Next, substituting $\tau(t) = 2(R_0 - vt)/c$ into the part of frequency difference in the above formula, we can get

$$\begin{aligned} s_b^{up}(t) &= \frac{1}{2}K_r A_0^2 \cos\{2\pi[(\frac{2kR_0}{c} + \frac{2kvT_1}{c} \\ &\quad - \frac{2f_0 v}{c})t - \frac{2kv}{c}t^2 + \frac{2f_0 R_0}{c} \\ &\quad - \frac{2kR_0 T_1}{c}] - \varphi_r\} \end{aligned} \tag{4}$$

According to Formula (4), we know that the center frequency and chirp rate of the beat signal can be expressed as

$$\begin{aligned} f_b^{up} &= \frac{2(kR_0 + kvT_1 - f_0 v)}{c} \\ k_b^{up} &= \frac{4kv}{c} \end{aligned} \tag{5}$$

Similarly, the beat signal of the lower sweep part can be obtained by mixing and filtering the corresponding transmit signal and echo signal. The formula can be expressed as

$$\begin{aligned} s_b^{down}(t) &= \frac{1}{2}K_r A_0^2 \cos\{2\pi[(\frac{2(2B+f_0)v}{c} \\ &\quad + \frac{2kR_0}{c} + \frac{2kvT_1}{c})t - \frac{2kv}{c}t^2 \\ &\quad - \frac{2(2B+f_0)R_0}{c} + \frac{2kR_0 T_1}{c}] - \varphi_r\} \end{aligned} \tag{6}$$

According to Formula (6), we know that the center frequency and chirp rate of beat signal can be expressed as

$$\begin{aligned} f_b^{down} &= \frac{2(2B+f_0)v}{c} + \frac{2kR_0}{c} + \frac{2kvT_1}{c} \\ k_b^{down} &= \frac{4kv}{c} \end{aligned} \tag{7}$$

After obtaining the beat signal corresponding to the upper sweep part and the lower sweep part, we can get the distance and speed information of the target, which can be expressed as

$$R_0 = \frac{c(f_b^{up} + f_b^{down})}{4k} \tag{8}$$

$$v = \frac{c(f_b^{down} - f_b^{up})}{4(f_0 + B)} \approx \frac{c(f_b^{down} - f_b^{up})}{4f_0} \tag{9}$$

III. POWER CONSUMPTION MODEL

Based on the previous section, to further analyze the power consumption performance of the SS-FMCW radar, we derive the power consumption model of traditional FMCW radar and SS-FMCW radar, and conduct in-depth comparative analysis from the theoretical dimension. In order to compare the differences between the two radars in terms of structure, we plot the differences between the two as shown in Fig. 2.

A. POWER CONSUMPTION MODEL OF THE TRADITIONAL FMCW RADAR

According to literature [12], [25], we know that the hardware composition of the traditional FMCW radar mainly includes a programmable frequency modulation signal transmission part and a programmable echo signal processing part. Correspondingly, the total power consumption of the radar is also composed of these two parts: transmitter power consumption and receiver power consumption. It should be noted that the power consumption involved in this section is average power consumption. Therefore, the total power consumption of the traditional FMCW radar can be expressed as

$$P_{\{all,1\}} = P_{\{t,1\}} + P_{\{r,1\}} \tag{10}$$

Specifically, the energy-consuming components of the traditional FMCW radar transmitter mainly include a microcomputer unit (MCU), a digital-to-analog converter (DAC), a voltage-controlled oscillator (VCO), a transmitting low noise power amplifier (T-PA). It should be noted that the power divider chosen in this paper is a passive component and does not consume energy. Then the power consumption of the transmitter can be expressed as

$$\begin{aligned} P_{\{t,1\}} = {} & P_{\{MCU,1\}} + P_{\{DAC,1\}} \\ & + P_{\{VCO,1\}} + P_{\{T-PA,1\}} \end{aligned} \tag{11}$$

where, $P_{\{MCU,1\}}$, $P_{\{DAC,1\}}$, $P_{\{VCO,1\}}$ and $P_{\{T-PA,1\}}$ represent the average power consumption of the MCU, the DAC, the VCO and the T-PA, respectively. Accordingly, the energy-consuming components of the receiver of the traditional FMCW radar mainly include a receiving low noise power amplifier (R-PA), a low-pass filter (LPF), an analog-to-digital converter (ADC), and a digital signal processing (DSP). It should be noted that the mixer selected in this paper is a passive component and does not consume energy. Then, the power consumption of the radar receiver can be expressed as

$$\begin{aligned} P_{\{r,1\}} = {} & P_{\{R-PA,1\}} + P_{\{LPF,1\}} \\ & + P_{\{ADC,1\}} + P_{\{DSP,1\}} \end{aligned} \tag{12}$$

where, $P_{\{R-PA,1\}}$, $P_{\{LPF,1\}}$, $P_{\{ADC,1\}}$ and $P_{\{DSP,1\}}$ represent the average power consumption of the R-PA, the LPF, the ADC and the DSP, respectively. Therefore, the total power consumption of the traditional FMCW radar can be expressed as

$$\begin{aligned} P_{\{all,1\}} &= P_{\{t,1\}} + P_{\{r,1\}} \\ &= P_{\{MCU,1\}} + P_{\{DAC,1\}} + P_{\{VCO,1\}} \\ &\quad + P_{\{T-PA,1\}} + P_{\{R-PA,1\}} \\ &\quad + P_{\{LPF,1\}} + P_{\{ADC,1\}} + P_{\{DSP,1\}} \end{aligned} \tag{13}$$

B. POWER CONSUMPTION MODEL OF THE SS-FMCW RADAR

Similar to the previous section, the total power consumption of the SS-FMCW radar includes transmitter power consumption and receiver power consumption. Then, the total power

$$s_t(t) = \begin{cases} A_0 \cos\{2\pi[f_0(t - nT - T_1) + \frac{k}{2}(t - nT - T_1)^2] + \varphi_0\}, \\ nT + T_1 \le t < (n+1)T - \frac{T_2}{2}, n = 0, 1, 2, \ldots \\ A_0 \cos\{2\pi[(2B + f_0)(t - nT - T_1) - \frac{k}{2}(t - nT - T_1)^2] + \varphi_0\}, \\ nT + T_1 + \frac{T_2}{2} \le t < (n+1)T, n = 0, 1, 2, \ldots \\ A_0 \cos(2\pi f_0 t + \varphi_0), other \end{cases} \tag{1}$$

$$s_r(t) = \begin{cases} K_r A_0 \cos\{2\pi[f_0(t - \tau(t) - nT - T_1) + \frac{k}{2}(t - \tau(t) - nT - T_1)^2] + \varphi_0 + \varphi_r\}, \\ nT + T_1 \le t < (n+1)T - \frac{T_2}{2}, n = 0, 1, 2, \ldots \\ K_r A_0 \cos\{2\pi[(2B + f_0)(t - \tau(t) - nT - T_1) - \frac{k}{2}(t - \tau(t) - nT - T_1)^2] + \varphi_0 + \varphi_r\}, \\ nT + T_1 + \frac{T_2}{2} \le t < (n+1)T, n = 0, 1, 2, \ldots \\ K_r A_0 \cos(2\pi f_0(t - \tau(t)) + \varphi_0 + \varphi_r), other \end{cases} \tag{2}$$

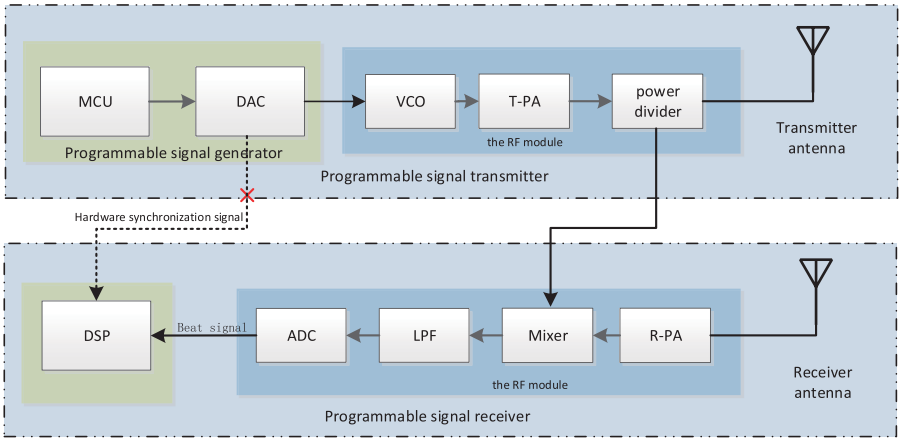

FIGURE 2. Structure diagram of the SS-FMCW radar.

consumption can be expressed as

$$P_{\{all,2\}} = P_{\{t,2\}} + P_{\{r,2\}} \tag{14}$$

The power consumption of the transmitter can be expressed as

$$\begin{aligned} P_{\{t,2\}} &= P_{\{MCU,2\}} + P_{\{DAC,2\}} \\ &\quad + P_{\{VCO,2\}} + P_{\{T-PA,2\}} \end{aligned} \tag{15}$$

where, $P_{\{MCU,2\}}$, $P_{\{DAC,2\}}$, $P_{\{VCO,2\}}$ and $P_{\{T-PA,2\}}$ represent the average power consumption of the MCU, the DAC, the VCO and the T-PA, respectively.

It shouldbe noted that according to the previous section, the intermittent ramp signal includes two parts in a cycle, the DC part and the ramp part (triangle wave part). The duration of these two parts is T_1 and T_2, respectively. Therefore, $P_{\{MCU,2\}}$, $P_{\{DAC,2\}}$, $P_{\{VCO,2\}}$ and $P_{\{T-PA,2\}}$ can be expressed as

$$\begin{aligned} \boldsymbol{p}_{\{t,2\}} &= [P_{\{MCU,2\}}, P_{\{DAC,2\}}, \\ P_{\{VCO,2\}}, P_{\{T-PA,2\}}]^T &= \begin{bmatrix} P_{M-dc} & P_{M-ram} \\ P_{D-dc} & P_{D-ram} \\ P_{V-dc} & P_{V-ram} \\ P_{T-P-dc} & P_{T-P-ram} \end{bmatrix} * \begin{bmatrix} \frac{T_1}{T} \\ \frac{T_2}{T} \end{bmatrix} \\ &= \begin{bmatrix} \frac{P_{M-dc}T_1 + P_{M-ram}T_2}{T} \\ \frac{P_{D-dc}T_1 + P_{D-ram}T_2}{T} \\ \frac{P_{V-dc}T_1 + P_{V-ram}T_2}{T} \\ \frac{P_{T-P-dc}T_1 + P_{T-P-ram}T_2}{T} \end{bmatrix} \end{aligned} \tag{16}$$

where, $\boldsymbol{p}_{\{t,2\}}$ is a column vector, P_{M-dc}, P_{D-dc}, P_{V-dc} and P_{T-P-dc} respectively represent the average power consumption of the MCU, the DAC, the VCO and the T-PA when processing the DC part, and P_{M-ram}, P_{D-ram}, P_{V-ram} and $P_{T-P-ram}$ respectively represent the average power consumption of the MCU, the DAC, the VCO and the T-PA when processing the ramp part. Correspondingly, the power consumption of the receiver can be expressed as

$$\begin{aligned} P_{\{r,2\}} &= P_{\{R-PA,2\}} + P_{\{LPF,2\}} \\ &\quad + P_{\{ADC,2\}} + P_{\{DSP,2\}} \end{aligned} \tag{17}$$

where, $P_{\{R-PA,2\}}$, $P_{\{LPF,2\}}$, $P_{\{ADC,2\}}$ and $P_{\{DSP,2\}}$ represent the average power consumption of the R-PA, the LPF, the ADC and the DSP, respectively. Similar to the transmitter part, the power consumption corresponding to the DC part and the power consumption corresponding to the ramp part need to be modeled separately.

$$\begin{aligned} \boldsymbol{p}_{\{r,2\}} &= [P_{\{R-PA,2\}}, P_{\{LPF,2\}}, \\ P_{\{ADC,2\}}, P_{\{DSP,2\}}]^T &= \begin{bmatrix} P_{R-P-dc} & P_{R-P-ram} \\ P_{L-dc} & P_{L-ram} \\ P_{A-dc} & P_{A-ram} \\ P_{DS-dc} & P_{DS-ram} \end{bmatrix} * \begin{bmatrix} \frac{T_1}{T} \\ \frac{T_2}{T} \end{bmatrix} \\ &= \begin{bmatrix} \frac{P_{R-P-dc}T_1 + P_{R-P-ram}T_2}{T} \\ \frac{P_{L-dc}T_1 + P_{L-ram}T_2}{T} \\ \frac{P_{A-dc}T_1 + P_{A-ram}T_2}{T} \\ \frac{P_{DS-dc}T_1 + P_{DS-ram}T_2}{T} \end{bmatrix} \end{aligned} \tag{18}$$

where, $\boldsymbol{p}_{\{r,2\}}$ is a column vector, P_{R-P-dc}, P_{L-dc}, P_{A-dc} and P_{DS-dc} respectively represent the average power consumption of the R-PA, the LPF, the ADC and the DSP when processing the DC part, and $P_{R-P-ram}$, P_{L-ram}, P_{A-ram} and P_{DS-ram} respectively represent the average power consumption of the R-PA, the LPF, the ADC and the DSP when processing the ramp part. In short, the total power consumption of the SS-FMCW radar can be expressed as

$$\begin{aligned} P_{\{all,2\}} &= P_{\{t,2\}} + P_{\{r,2\}} \\ &= P_{\{MCU,2\}} + P_{\{DAC,2\}} + P_{\{VCO,2\}} \\ &\quad + P_{\{T-PA,2\}} + P_{\{R-PA,2\}} + P_{\{LPF,2\}} \\ &\quad + P_{\{ADC,2\}} + P_{\{DSP,2\}} \\ &= \sum_{i=0}^{3} \boldsymbol{p}_{\{t,2,i\}} + \sum_{i=0}^{3} \boldsymbol{p}_{\{r,2,i\}} \\ &= \frac{P_\alpha T_1 + P_\beta T_2}{T} \end{aligned} \tag{19}$$

where, $\boldsymbol{p}_{\{t,2,i\}}$ or $\boldsymbol{p}_{\{r,2,i\}}$ is the i-th element in the vector, P_α represents the total power consumption of each

component of the SS-FMCW radar in processing DC part, P_β represents the total power consumption of each component of the SS-FMCW radar in processing ramp part.

IV. THEORETICAL ANALYSIS OF POWER CONSUMPTION PERFORMANCE

To facilitate the analysis of the difference in power consumption performance between the traditional FMCW radar and the SS-FMCW radar, the ratio of total power consumption between them is defined as Q_p, and the specific formula is as follows

$$Q_p = \frac{P_{\{all,1\}}}{P_{\{all,2\}}} = \frac{P_{\{all,1\}}T}{P_\alpha T_1 + P_\beta T_2} \tag{20}$$

In order to more intuitively reflect the power consumption performance advantages of the SS-FMCW radar and its relationship with $T_1$and T_2, the ratio of T_1 to T is defined as the duty cycle factor D_p, and formula (20) can be expressed as

$$Q_p = \frac{P_{\{all,1\}}}{(P_\alpha - P_\beta)D_p + P_\beta} \tag{21}$$

According to practical physical principles, Q_p, $P_{\{all,1\}}$, P_α, P_β, T, T_1, T_2 and D_p are positive numbers, and $0 \le D_p \le 1$. Therefore, we can get

1) When $P_\alpha = P_\beta$, Q_p is not related to D_p.
2) When $P_\alpha > P_\beta$, if $D_p = \frac{P_{\{all,1\}}-P_\beta}{P_\alpha-P_\beta}$ and $0 \le D_p \le 1$, the power consumption performance of the SS-FMCW radar is consistent with that of the traditional FMCW radar; if $D_p > \frac{P_{\{all,1\}}-P_\beta}{P_\alpha-P_\beta}$ and $0 \le D_p \le 1$, the power consumption performance of the traditional FMCW radar is better than that of the SS-FMCW radar, and the performance advantage is more obvious with the increase of D_p value; if $D_p < \frac{P_{\{all,1\}}-P_\beta}{P_\alpha-P_\beta}$ and $0 \le Dp \le 1$, the power consumption performance of the SS-FMCW radar is better than that of the traditional FMCW radar, and the performance advantage is more obvious with the decrease of D_p value.
3) When $P_\alpha < P_\beta$, if $D_p = \frac{P_{\{all,1\}}-P_\beta}{P_\alpha-P_\beta}$ and $0 \le D_p \le 1$, the power consumption performance of the SS-FMCW radar is consistent with that of the traditional FMCW radar; if $D_p < \frac{P_{\{all,1\}}-P_\beta}{P_\alpha-P_\beta}$ and $0 \le D_p \le 1$, the power consumption performance of the traditional FMCW radar is better than that of the SS-FMCW radar, and the performance advantage is more obvious with the decrease of D_p value; if $D_p > \frac{P_{\{all,1\}}-P_\beta}{P_\alpha-P_\beta}$ and $0 \le Dp \le 1$, the power consumption performance of the SS-FMCW radar is better than that of the traditional FMCW radar, and the performance advantage is more obvious with the increase of D_p value.

V. EXPERIMENTAL RESULTS AND ANALYSIS

In order to validate the theoretical analysis of radar power performance in the previous section, this section analyzes the differences in power performance between the traditional FMCW radar and the SS-FMCW radar through simulations and measurements. In the experiment, the two radars use the same components and are built according to the structure of Fig. 2 (a) and (b), respectively. In addition, the modulation signal of the traditional FMCW radar is a triangle wave signal, as shown in Fig. 3 (a), and the modulation signal of the SS-FMCW radar is an intermittent triangle wave signal, as shown in Fig. 3 (b).

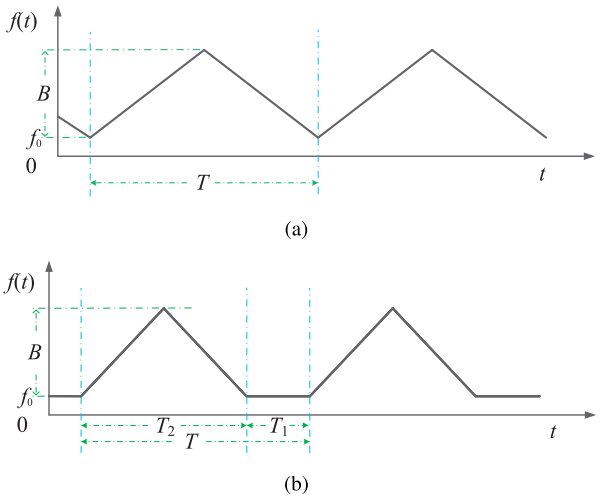

FIGURE 3. (a) Triangle wave signal; (b) Intermittent triangle wave signal.

TABLE 1. Typical power consumption of each component.

	Name	Typical power consumption
Transmitter	MCU	0.792mW
	DAC	18mW
	VCO	225mW
	T-PA	275mW
Receiver	R-PA	275mW
	LPF	20mW
	ADC	15mW
	DSP	Work mode: 627mW Sleep mode: 23mW

A. SIMULATION EXPERIMENT RESULTS AND ANALYSIS

In order to verify the theoretical analysis in the previous section, the simulation experiment in this section mainly includes: (1) The total power consumption of the traditional FMCW radar; (2) The total power consumption of the SS-FMCW radar; (3) The relationship between the ratio of total power consumption Q_p, duty cycle factor D_p and modulation signal cycle T. In addition, the typical power consumption of radar components during the experiment can refer to data sheets [27], [28], [29] (Mini-Circuits, TEXAS INSTRUMENTS and ANALOG DEVICES), as shown in Table 1.

During the experiment, the typical power consumption of each radar component is shown in Table 1. The SS-FMCW radar used in this paper operates in the 2.4 GHz band, so the power consumption values of the various components of the radar are typical for this band. It should be noted that the DSP of the SS-FMCW radar can enter a sleep mode when processing the DC part to reduce its power consumption. In addition, the value of D_p is set as $0 \le D_p \le 1$, and the value of T is set as $0 \le T \le 100$ms. The final experimental results are shown in Fig. 4.

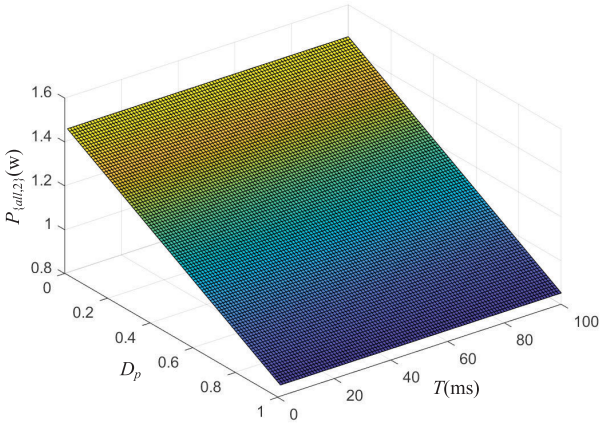

(a)

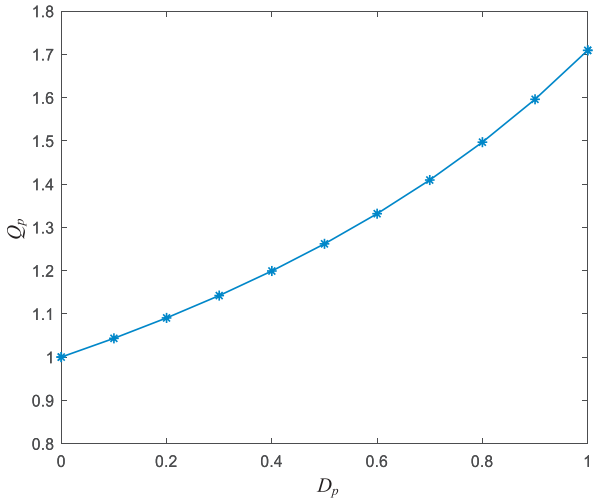

(b)

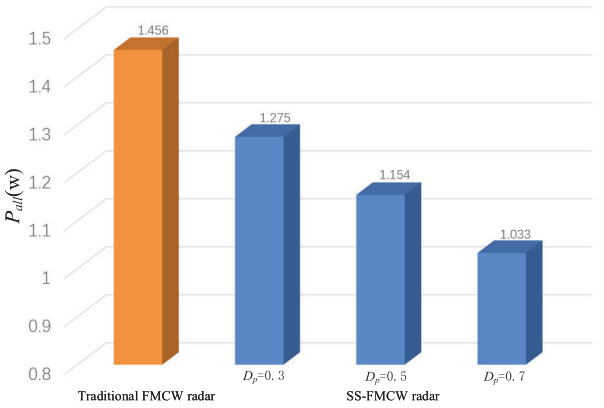

(c)

FIGURE 4. (a) The change of $P_{\{all,2\}}$ with D_p and T; (b) The change of Q_p with D_p; (c) Comparison diagram of total power consumption of radars.

According to the experimental results, we know that $P_\alpha < P_\beta$ and $P_{\{all,1\}} = P_\beta$, which belongs to the last case in the theoretical analysis. The total power consumption of the SS-FMCW radar will decrease with increasing D_p value for a given T value, but will not vary with T value for a given D_p value. The total power consumption ratio Q_p of the traditional

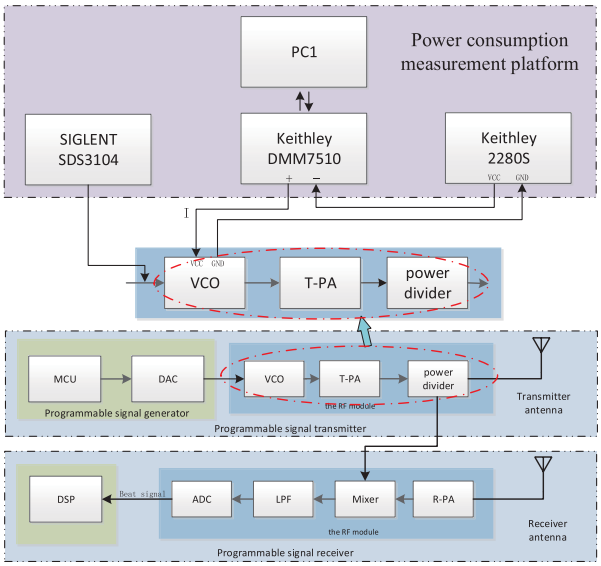

FIGURE 5. Block diagram of power consumption measurement platform.

FMCW radar and the SS-FMCW radar will increase with the value of D_p and will always be not less than one. In other words, when $D_p > 0$, the power consumption performance of the SS-FMCW radar is always better than that of the traditional FMCW radar, and with the increase of D_p value, the power consumption performance advantage is more obvious. Specifically, when $D_p = 0.5$, the power consumption of the former is 20.7% lower than that of the latter. Therefore, the simulation results in this section are consistent with the theoretical analysis in the previous section.

B. ACTUAL EXPERIMENT RESULTS AND ANALYSIS

To further verify the theoretical analysis in the previous section, this section will take the components selected in this paper as an example of actual testing. Furthermore, we analyze the difference in power consumption performance between the traditional FMCW radar and the SS-FMCW radar. The block diagram of the power consumption measurement platform (take the VCO as an example) is shown in Fig. 5.

The platform includes SIGLENT SDS3104 (an oscilloscope), Keithley DMM7510 (a high-precision graphic sampling multimeter), Keithley 2280S (a high-precision measuring DC power), PC1 and PC2. As an example, during the VCO power consumption test, the VCO, the Keithley DMM7510 and the Keithley 2280S form a series circuit, as shown in Fig. 5. The Keithley 2280S is used to supply power to the VCO, and the output voltage is 5V. The Keithley DMM7510 is used to measure and collect the instantaneous current in the circuit, and transmit the collected current values to PC1. The SIGLENT SDS3104 is used to monitor the signal waveform. Based on this, we test the instantaneous working voltage and current of each radar component when processing the DC signals and ramp signals.

According to the acquisition results, we know that the instantaneous current of each component of the radar when processing DC signals is slightly less than that when

TABLE 2. Average power consumption of each component.

Components	Average power consumption (Triangle signal)		Average power consumption (DC signal)	
	I(mA)	P(mW)	I(mA)	P(mW)
MCU	17.17	85.85	16.42	82.10
DAC	3.29	16.45	2.81	14.05
VCO	36.17	180.85	35.31	176.55
T-PA	52.56	262.80	52.51	262.55
R-PA	76.76	383.80	77.76	388.80
LPF	12.28	61.40	12.13	60.65
ADC	32.45	162.25	32.50	162.50

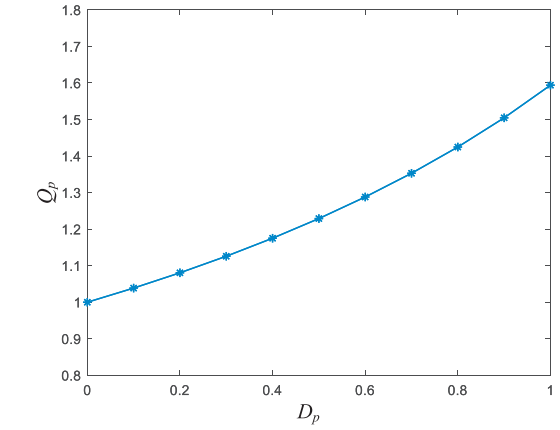

(a)

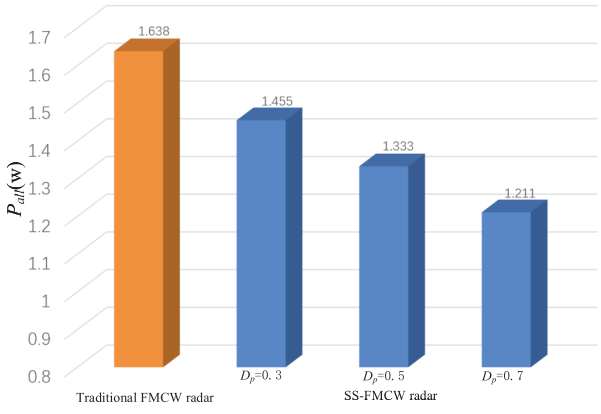

(b)

FIGURE 6. (a) The change of Q_p with D_p; (b) Comparison diagram of total power consumption of radars.

processing slope signals. In order to study the average power consumption of each component more intuitively, we calculate the average power consumption of each component of the radar, as shown in Table 2. Considering that the DSP in this paper is a PC, its instantaneous working current and voltage are difficult to measure accurately. Therefore, the typical power consumption value is selected in the subsequent analysis. In addition, B is set to 226.6MHz and f_0 is set to 2.4GHz, and the experimental results are shown in Fig. 6.

According to the experimental results, we know that $P_\alpha < P_\beta$ and $P_{\{all,1\}} = P_\beta$, which belongs to the last case in the theoretical analysis. The actual test results are similar to the simulation results in the previous section. The total power consumption ratio Q_p will increase with the value of D_p and will never be less than one. In other words, the power performance of the SS-FMCW radar is much better than that of the traditional FMCW radar when $D_p > 0$, and the power performance advantage becomes more obvious as the value of D_p increases. Specifically, when $D_p = 0.5$, the power consumption of the former is 18.6% lower than that of the latter. The deviation of the actual test results from the simulation results is due to the deviation of the average values of the power consumption of the components selected in this paper from the typical values in the data sheets. Therefore, the actual results in this section are consistent with the theoretical analysis in the previous section.

VI. CONCLUSION

This article fills the blank of power consumption performance analysis of the SS-FMCW radar. Specifically, we analyze the principle behind the SS-FMCW radar based on intermittent ramp signals. Based on this, we propose a module level power consumption model for the SS-FMCW radar. Furthermore, we propose a duty cycle factor, and compare the power consumption performance difference between the traditional FMCW radar and the SS-FMCW radar under different factor values. Finally, the experimental results show that the SS-FMCW radar is superior to the conventional FMCW radar in terms of power consumption performance. Especially, when $D_p = 0.5$, the former is 18.6% lower than the latter in the actual test experiment. In future work, we will further explore the power consumption performance of the SS-FMCW radar in specific application scenarios, such as the automotive sector.

REFERENCES

[1] Z. Wang, G. Li, and L. Yang, "Dynamic hand gesture recognition based on micro-Doppler radar signatures using hidden Gauss–Markov models," *IEEE Geosci. Remote Sens. Lett.*, vol. 18, no. 2, pp. 291–295, Feb. 2021.

[2] Y. Zhang, S. Dong, C. Zhu, M. Balle, B. Zhang, and L. Ran, "Hand gesture recognition for smart devices by classifying deterministic Doppler signals," *IEEE Trans. Microw. Theory Techn.*, vol. 69, no. 1, pp. 365–377, Jan. 2021.

[3] K. Han and S. Hong, "Vocal signal detection and speaking-human localization with MIMO FMCW radar," *IEEE Trans. Microw. Theory Techn.*, vol. 69, no. 11, pp. 4791–4802, Nov. 2021.

[4] F. Liang, H. Lou, Y. Zhang, H. Lv, X. Yu, Q. An, Z. Li, and J. Wang, "Through-the-wall high-dimensional imaging of human vital signs by combining multiple enhancement algorithms using portable LFMCW-MIMO radar," *Measurement*, vol. 195, May 2022, Art. no. 111074.

[5] P. Chen, S. Guo, H. Li, X. Wang, G. Cui, C. Jiang, and L. Kong, "Through-wall human motion recognition based on transfer learning and ensemble learning," *IEEE Geosci. Remote Sens. Lett.*, vol. 19, pp. 1–5, 2022.

[6] A. Kumar, Z. Li, Q. Liang, B. Zhang, and X. Wu, "Experimental study of through-wall human detection using ultra wideband radar sensors," *Measurement*, vol. 47, pp. 869–879, Jan. 2014.

[7] S. Zhu, R. G. Guendel, A. Yarovoy, and F. Fioranelli, "Continuous human activity recognition with distributed radar sensor networks and CNN–RNN architectures," *IEEE Trans. Geosci. Remote Sens.*, vol. 60, 2022, Art. no. 5115215.

[8] X. Li, Y. He, F. Fioranelli, X. Jing, A. Yarovoy, and Y. Yang, "Human motion recognition with limited radar micro-Doppler signatures," *IEEE Trans. Geosci. Remote Sens.*, vol. 59, no. 8, pp. 6586–6599, Aug. 2021.
[9] X. Dong, Z. Zhao, Y. Wang, T. Zeng, J. Wang, and Y. Sui, "FMCW radar-based hand gesture recognition using spatiotemporal deformable and context-aware convolutional 5-D feature representation," *IEEE Trans. Geosci. Remote Sens.*, vol. 60, pp. 1–11, 2022.
[10] B. Li, J. Yang, Y. Yang, C. Li, and Y. Zhang, "Sign language/gesture recognition based on cumulative distribution density features using UWB radar," *IEEE Trans. Instrum. Meas.*, vol. 70, pp. 1–13, 2021.
[11] J. W. Smith, S. Thiagarajan, R. Willis, Y. Makris, and M. Torlak, "Improved static hand gesture classification on deep convolutional neural networks using novel sterile training technique," *IEEE Access*, vol. 9, pp. 10893–10902, 2021.
[12] T. Wang, P. Li, M. Wang, D. Yang, and C. Shi, "A flexible, efficient and low-cost experimental platform for FMCW radars," *Sensor Rev.*, vol. 39, no. 4, pp. 495–503, Jul. 2019.
[13] T. Wang, P. Li, R. Wang, Z. Sheng, and L. Huang, "A software-synchronization based, flexible, low-cost FMCW radar," *IEEE Access*, vol. 8, pp. 115582–115592, 2020.
[14] J. Yan, H. Liu, B. Jiu, and Z. Bao, "Power allocation algorithm for target tracking in unmodulated continuous wave radar network," *IEEE Sensors J.*, vol. 15, no. 2, pp. 1098–1108, Feb. 2015.
[15] C. Shi, F. Wang, M. Sellathurai, J. Zhou, and S. Salous, "Power minimization-based robust OFDM radar waveform design for radar and communication systems in coexistence," *IEEE Trans. Signal Process.*, vol. 66, no. 5, pp. 1316–1330, Mar. 2018.
[16] C. Shi, Y. Wang, F. Wang, S. Salous, and J. Zhou, "Joint optimization scheme for subcarrier selection and power allocation in multicarrier dual-function radar-communication system," *IEEE Syst. J.*, vol. 15, no. 1, pp. 947–958, Mar. 2021.
[17] K. B. Cooper, R. Rodriguez Monje, R. J. Dengler, C. J. Cochrane, M. Alonso-Delpino, A. Tang, T. O. El Bouayadi, and O. Pradhan, "A compact, low power consumption, and highly sensitive 95 GHz Doppler radar," *IEEE Sensors J.*, vol. 20, no. 11, pp. 5865–5875, Jun. 2020.
[18] H. Zhang, W. Liu, B. Zong, J. Shi, and J. Xie, "An efficient power allocation strategy for maneuvering target tracking in cognitive MIMO radar," *IEEE Trans. Signal Process.*, vol. 69, pp. 1591–1602, 2021.
[19] Y. Shi, B. Jiu, J. Yan, H. Liu, and K. Li, "Data-driven simultaneous multibeam power allocation: When multiple targets tracking meets deep reinforcement learning," *IEEE Syst. J.*, vol. 15, no. 1, pp. 1264–1274, Mar. 2021.
[20] Y. Shi, B. Jiu, J. Yan, and H. Liu, "Data-driven radar selection and power allocation method for target tracking in multiple radar system," *IEEE Sensors J.*, vol. 21, no. 17, pp. 19296–19306, Sep. 2021.
[21] J. Yan, W. Pu, H. Liu, B. Jiu, and Z. Bao, "Robust chance constrained power allocation scheme for multiple target localization in colocated MIMO radar system," *IEEE Trans. Signal Process.*, vol. 66, no. 15, pp. 3946–3957, Aug. 2018.
[22] T. Tian, G. Li, and T. Zhou, "Power distribution for an OFDM-based dual-function radar-communication sensor," *IEEE Sensors Lett.*, vol. 4, no. 11, pp. 1–4, Nov. 2020.
[23] C. Latham, A. Egbert, C. Baylis, L. Cohen, and R. J. Marks, "Joint radar amplifier circuit and waveform optimization for ambiguity function, power-added efficiency, and spectral compliance," *IEEE Trans. Aerosp. Electron. Syst.*, vol. 55, no. 3, pp. 1190–1199, Jun. 2019.
[24] P. Li, T. Wang, R. Wang, Y. Sun, Y. Wu, and L. Huang, "FFBV algorithm design for soft synchronization FMCW radar," *IEEE Trans. Instrum. Meas.*, vol. 70, pp. 1–11, 2021.
[25] P. Li, T. Wang, R. Wang, Y. Wu, and Y. Sun, "Energy-efficiency strategy for soft synchronization FMCW radar," *IEEE Trans. Instrum. Meas.*, vol. 71, pp. 1–11, 2022.
[26] M. A. Richards, J. Scheer, W. A. Holm, and W. L. Melvin, *Principles of Modern Radar*. Raleigh, NC, USA: SciTech, 2010.
[27] Mini-Circuits. (2023). [Online]. Available: https://www.minicircuits.com/products
[28] Texas Instruments. (2023). *Microcontrollers and Processors*. [Online]. Available: https://www.ti.com.cn/zh-cn/microcontrollers-mcus-processors/products
[29] (2023). *Analog Devices*. [Online]. Available: https://www.ti.com.cn/zh-cn/microcontrollers-mcus-processors/products

PING LI received the B.E. degree in electronic and information engineering from Hangzhou Dianzi University, Hangzhou, China, in 2017, and the Ph.D. degree in communication and information systems from Shanghai University, in 2019.

He is currently a Lecturer with Hangzhou Dianzi University. His current research interests include radar signal processing and target detection.

TAO WANG (Senior Member, IEEE) received the first Ph.D. degree from Zhejiang University, China, in 2006, and the second Ph.D. degree from Université Catholique de Louvain (UCL), Belgium, in 2012.

Since February 2013, he has been a Professor with Shanghai University. His current interest includes signal processing and control techniques for wireless systems. He was an Associate Editor of *EURASIP Journal on Wireless Communications and Networking*.